FRONTIERS OF PHYSICS

RESEARCH ARTICLE
Volume 19 / Issue 2 / 22202 / 2024

Two-dimensional anisotropic vortex quantum droplets in dipolar Bose–Einstein condensates

Guilong Li[1], Xunda Jiang[1], Bin Liu[1,†], Zhaopin Chen[2], Boris A. Malomed[3,4], Yongyao Li[1,5,‡]

1 School of Physics and Optoelectronic Engineering, Foshan University, Foshan 528225, China
2 Physics Department and Solid-State Institute, Technion, Haifa 32000, Israel
3 Department of Physical Electronics, School of Electrical Engineering, Faculty of Engineering, Tel Aviv University, Tel Aviv 69978, Israel
4 Instituto de Alta Investigación, Universidad de Tarapacá, Casilla 7D, Arica, Chile
5 Guangdong-Hong Kong-Macao Joint Laboratory for Intelligent Micro-Nano Optoelectronic Technology, Foshan University, Foshan 528225, China
Corresponding authors. E-mail: †bin-liu@fosu.edu.cn, ‡yongyaoli@gmail.com
Received August 10, 2023; accepted August 21, 2023

ABSTRACT

Creation of stable intrinsically anisotropic self-bound states with embedded vorticity is a challenging issue. Previously, no such states in Bose–Einstein condensates (BECs) or other physical settings were known. Dipolar BEC suggests a unique possibility to predict stable two dimensional anisotropic vortex quantum droplets (2D-AVQDs). We demonstrate that they can be created with the vortex axis oriented *perpendicular* to the polarization of dipoles. The stability area and characteristics of the 2D-AVQDs in the parameter space are revealed by means of analytical and numerical methods. Further, the rotation of the polarizing magnetic field is considered, and the largest angular velocities, up to which spinning 2D-AVQDs can follow the rotation in clockwise and anti-clockwise directions, are found. Collisions between moving 2D-AVQDs are studied too, demonstrating formation of bound states with a vortex–antivortex–vortex structure. A stability domain for such stationary bound states is identified. Unstable dipolar states, that can be readily implemented by means of phase imprinting, quickly transform into robust 2D-AVQDs, which suggests a straightforward possibility for the creation of these states in the experiment.

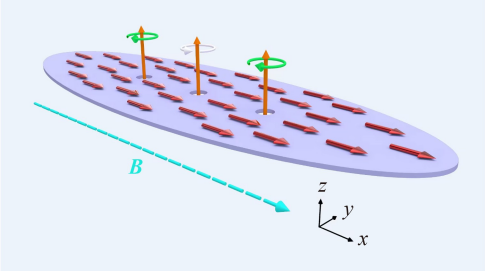

Keywords dipolar Bose–Einstein condensate, anisotropic vortex quantum droplets

1 Introduction

Nonlocal nonlinearities underlie remarkable phenomena in diverse fields. In particular, while two and three-dimensional (2D and 3D) self-trapped modes, supported by the ubiquitous local cubic self-attraction, are unstable due to the occurrence of the critical and supercritical collapse in the same settings [1–3], the nonlocal nonlinearity arrests the onset of the collapse, thus stabilizing the 2D and 3D solitons [4, 5]. In Bose–Einstein condensates (BECs), stable 2D and 3D matter-wave solitons were predicted in free space, making use of long-range van der Waals interactions between Rydberg atoms [6, 7] or laser-induced artificial gravity [8], microwave-coupled

Higher Education Press

arXiv: 2301.04305
https://doi.org/10.1007/s11467-023-1338-7

binary condensates [9], and dipole–dipole interactions (DDIs) [10–15]. Unlike other nonlocal interactions, DDIs feature strong anisotropy in 3D, while in the 2D geometry DDIs are isotropic or anisotropic if the dipoles are polarized, respectively, perpendicular to the system's plane or making an angle $< 90^{\circ}$ with it.

The stability of 2D and 3D self-trapped modes with embedded vorticity is a challenging problem. Solitary vortices are often subject to the azimuthal modulational instability that develops faster than the collapse, splitting the vortices into fragments [5]. The nonlocality can help to suppress the splitting instability if, roughly speaking, the wavelength of the azimuthal perturbations is smaller than the nonlocality scale. In BEC, stable vortex solitons supported by nonlocal interactions were predicted for Rydberg atoms in 3D [16], microwave-coupled binary BECs [9], and dipolar BECs with specially arranged isotropic DDIs in 2D [17]. All these modes featuring isotropic shapes, an open question is whether anisotropic ones with embedded vorticity (topological charge) may be made stable in the free space. Anisotropic DDIs offer a possibility to construct them. In particular, spin–orbit coupling (SOC) has helped to predict stable anisotropic solitons mixing fundamental (zero-vorticity) and vortex components in the spinor–dipolar BEC [18–20]. However, vortex components play a subordinate role in the SOC system, carrying a small part of the soliton's norm.

Recently, 3D self-bound states in dipolar BECs were observed in the form of quantum droplets (QDs), stabilized by the beyond-mean-field (MF) effect, which is represented by the Lee–Huang–Yang (LHY) term in the respective Gross–Pitaevskii equation (GPE) [21, 22]. The experimentally demonstrated QDs feature a strong anisotropy in their density profile in the free space, but they do not carry vorticity. Their counterparts in the form of isotropic QDs were experimentally created in quasi-2D [23] and 3D [24, 25] forms in binary BECs with intercomponent attraction, as predicted by Petrov [26]. The stability and shapes of these self-trapped quantum-fluid states are determined by the competition between the MF and LHY nonlinearities [27–30].

The LHY-enhanced BEC setting is favorable for stabilizing self-bound vortex modes. Isotropic 2D and 3D vortex QDs in the free-space binary BEC have been predicted to be stable with topological charges $S \leq 5$ [31] and $S \leq 2$ [32], respectively. Stable semi-discrete vortex QDs, also with $S \leq 5$, were predicted in an array of tunnel-coupled quasi-1D potential traps [33].

For the dipolar QDs, isotropic vortex solutions with the dipoles polarized parallel to the vortical pivot were constructed and found to be completely unstable [34]. Hence the inability to create stable vortex modes in dipolar QDs remains a fundamental and unresolved problem. The aim of this work is to address this problem, considering dipolar vortex QDs in the 2D geometry with dipoles polarized parallel to the plane in which the vortex structure is formed, and the vortex axis being perpendicular to the plane and the polarization. Compared to previously studies vortex QDs in dipolar and binary systems, in the current setting their shape is strongly anisotropic, breaking the rotational symmetry with respect to the vorticity axis. Previously, no example of stable anisotropic vortex states was predicted in any model.

2 Model and stationary solutions

Dynamics of the system is governed by the scaled form of the 2D GPE with the LHY correction:

$$\mathrm{i}\frac{\partial}{\partial t}\psi = \left[-\frac{1}{2}\nabla^2 + \Phi_{\mathrm{dd}}(\boldsymbol{r}) + g|\psi|^2 + \gamma|\psi|^3\right]\psi, \tag{1}$$

where strengths of the local MF and LHY self-repulsion are [35], respectively, $g > 0$ and

$$\gamma = \frac{4g^{5/2}}{3\pi^2}\left(1 + \frac{8\pi^2}{3g^2}\right) > 0. \tag{2}$$

The DDI is represented by term $\Phi_{\mathrm{dd}}(\boldsymbol{r}) = \int R(\boldsymbol{r}-\boldsymbol{r}')|\psi(\boldsymbol{r}')|^2\mathrm{d}\boldsymbol{r}'$, with the interaction kernel [36, 37]

$$R(\boldsymbol{r}-\boldsymbol{r}') = \frac{1-3\cos^2\Theta}{[b^2+(\boldsymbol{r}-\boldsymbol{r}')^2]^{3/2}}. \tag{3}$$

This kernel implies that, as said above, all dipoles are polarized along the x-direction in the 2D plane, i.e., $\cos^2\Theta = (x-x')^2/|\boldsymbol{r}-\boldsymbol{r}'|^2$, and cutoff scale b is determined by the thickness of the BEC layer in the third direction. In this case, the anisotropic DDIs are chiefly attractive.

Stationary solutions are looked for in the usual form, $\psi(\boldsymbol{r},t) = \phi(\boldsymbol{r})\mathrm{e}^{-\mathrm{i}\mu t}$, with wave function $\phi(\boldsymbol{r})$ and real chemical potential μ. Dynamical invariants of the system are the total norm and momentum

$$N = \int |\phi(\boldsymbol{r})|^2\mathrm{d}\boldsymbol{r}, \quad \boldsymbol{P} = \mathrm{i}\int \psi\nabla\psi^*\mathrm{d}\boldsymbol{r},$$

where N is proportional to the number of atoms in the dipolar BEC, and its energy

$$E = \frac{1}{2}\int \mathrm{d}\boldsymbol{r}\left[|\nabla\psi|^2 + g|\psi|^4 + \Phi_{\mathrm{dd}}(\boldsymbol{r})|\psi|^2 + \frac{4}{5}\gamma|\psi|^5\right]. \tag{4}$$

2D-AVQDs with integer vorticity S are produced in the numerical form by means of the imaginary-time method (ITM), initiated by an anisotropic ansatz,

$$\phi^{(0)}(x,y) = A\tilde{r}^S\exp\left(-\alpha\tilde{r}^2 + \mathrm{i}S\tilde{\theta}\right), \tag{5}$$

where A and α are positive constants, and $\left\{\tilde{r},\tilde{\theta}\right\} \equiv \left\{\sqrt{x^2+\beta^2y^2}, \arctan(\beta y/x)\right\}$ with an anisotropy factor $\beta > 1$. In this work we set $b = 1$ by rescaling and

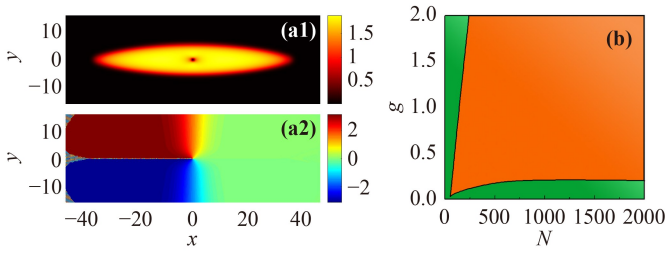

Fig. 1 **(a1, a2)** A typical example of stable 2D-AVQDs, with $(N, g) = (1000, 0.25)$. The panels (a1, a2) display, severally, density and phase patterns of the droplet. **(b)** In the plane of (N, g), 2D-AVQDs ($S = 1$), fundamental QDs ($S = 0$) are stable in the orange area. In the green area, only dipole mode and fundamental QDs can be stable.

fix $\beta = 2$, using N and g as control parameters. Note that the vorticity may be defined, as per Eq. (5), in spite of the lack of axial symmetry and nonconservation of the angular momentum.

A typical example of numerically found stable 2D-AVQDs with $S = 1$ is produced in Figs. 1(a1, a2). Their stability area is summarized in the (N, g) plane, plotted in Fig. 1(b). In particular, the stable 2D-AVQDs are found at $N > N_{\min}$, where $N_{\min}$ is a gradually increasing function of g. At $N < N_{\min}$, the vortex ansatz produces stable dipole modes. For fixed N, stable 2D-AVQDs are found at $g > g_{\min}(N)$. At values of g slightly smaller than $g_{\min}$, the 2D-AVQDs starts spontaneous drift, keeping its topological charge. Deeper into the region of $g < g_{\min}$, the unstable 2D-AVQDs quickly decay to the fundamental QDs. The dipole modes produced by the dipole ansatz in the orange region of Fig. 1(b) are unstable. In the course of the perturbed real-time evolution, they spontaneously transform into stable vortices, suggesting a feasible scenario for the creation of the vortex modes in the experiment, as discussed in detail below.

The instability of 3D isotropic vortices, with dipoles polarized parallel to the vorticity axis [34], is explained by the fact the void around the long axis implies effective removal of a tube filled by dipoles which chiefly attract each other, i.e., removal of a large amount of the negative interaction energy (in other words, addition of a positive energy, which naturally leads to the destabilization). On the contrary to that, the present configuration, with the mutually perpendicular vorticity and in-plane polarization, stability is feasible because the void occupies an area around the vortex' pivot, where the DDIs overall display repulsion, thus removing some positive energy.

The stability was tested by real-time evolution with the perturbed noises. The time should exceed the respective diffraction time, at least, by an order of magnitude, be larger than $10 \times 2R^2$, where R is the radial size of the droplets. For example, in Figs. 1(a1) and 5(a1), the radial sizes of the 2D-AVQDs and the vortex–antivortex –vortex self-bound state are $R \sim 30$ and 40, respectively, while the corresponding simulation times are $\simeq 18000$ and 32000. The stability and instability of the 2D-AVQDs and dipole states, identified by means of direct simulations, was corroborated by numerical computation of eigenvalues for small perturbations around the stationary states, governed by the linearized Bogoliubov–de Gennes (BdG) equations. For the stable 2D-AVQDs, the BdG solution reveals the existence of an intrinsic perturbation eigenmode. In particular, for the state shown in Figs. 1(a1, a2), the eigenfrequency of the internal mode is 0.5. Detailed analysis of the respective excited states of 2D-AVQDs will be reported elsewhere.

For stationary QDs with a large norm, one can apply the analytical Thomas–Fermi (TF) approximation, neglecting the kinetic-energy term in Eq. (1). Then, the QD density, n, determines the total energy (4) as

$$E = \frac{1}{2}\left[(\varepsilon + g)n^2 + \frac{4}{5}\gamma n_e^{5/2}\right] A, \tag{6}$$

where $A = N/n$ is the area of the QDs, and $\varepsilon = \int \mathrm{d}\boldsymbol{r} R(\boldsymbol{r}) \approx -3.23$ represents the nonlocality effect. The equilibrium density, n_e, is the value providing an energy minimum as $\mathrm{d}E/\mathrm{d}n = 0$, which yields

$$\sqrt{n_e} = -\frac{5}{6\gamma}(\varepsilon + g), \quad A_e = \frac{36}{25}\gamma^2 \frac{N}{(\varepsilon + g)^2}. \tag{7}$$

An obvious condition, $\sqrt{n_e} > 0$, applied to Eq. (7), leads to $g < g_{\max} \equiv -\varepsilon \approx 3.23$. At $g > g_{\max}$, the strong local repulsion overcomes the effective nonlocal attraction, hence no self-bound state can be formed. Actually, n_e becomes very small and the size of 2D-AVQDs very large at $g > 2$, which makes it difficult to reach $g_{\max}$ in the numerical solution. The chemical potential corresponding to density [Eq. (7)] is

$$\mu_e = (\varepsilon + g)n_e + \gamma n_e^{3/2}. \tag{8}$$

These analytical predictions are compared to numerical findings in Figs. 2(a1–a3, b1–b3).

To characterized 2D-AVQDs families, we define their effective area, aspect ratio, and average angular momentum:

$$A_{\mathrm{eff}} = \frac{\left(\int |\phi|^2 \mathrm{d}\boldsymbol{r}\right)^2}{\int |\phi|^4 \mathrm{d}\boldsymbol{r}}, \mathcal{E}_l = \frac{W_y}{W_x}, \bar{L}_z = \int \frac{\phi^* \hat{L}_z \phi}{N} \mathrm{d}\boldsymbol{r}, \tag{9}$$

where $W_y \equiv \left(\int |\phi(x=0,y)|^2 \mathrm{d}y\right)^2 / \int |\phi(x=0,y)|^4 \mathrm{d}y$, $W_x \equiv \left(\int |\phi(x,y=0)|^2 \mathrm{d}x\right)^2 / \int |\phi(x,y=0)|^4 \mathrm{d}x$, and $\hat{L}_z = -\mathrm{i}(x\partial_y - y\partial_x)$. Figure 2 displays these quantities, along with $I_{\mathrm{P}} = |\phi|^2_{\max}$ and μ, versus N and g in the stability area. In panel 2(a1), the peak value saturates at $(I_{\mathrm{P}})_{\mathrm{sat}} \approx 1.938$ if N is sufficiently large, as expected for an incompressible quantum fluid. Panel 2(a2) shows that the chemical potential satisfies the Vakhitov–Kolokolov (VK) criterion, $\mathrm{d}\mu/\mathrm{d}N < 0$, which is the well-known necessary stability condition for self-trapped modes [1–3, 38]. For large N the chemical potential saturates at $\mu \approx -0.889$.

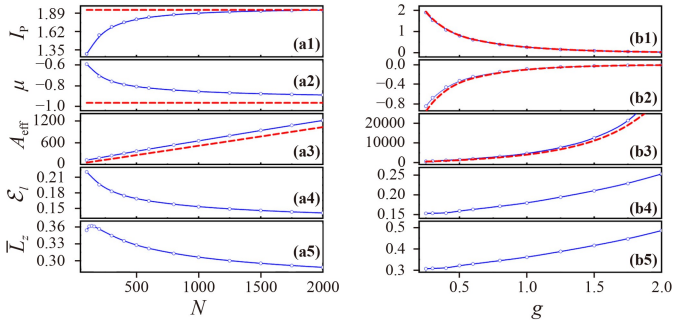

Fig. 2 The peak density (I_P), chemical potential (μ), effective area ($A_{\rm eff}$), aspect ratio ($\mathcal{E}_l$), and average angular momentum ($\bar{L}_z$), see Eq. (9), vs. N **(a1–a5)** and g **(b1–b5)**. In panels (a1–a5), $g = 0.25$ is fixed, while in panels (b1–b5) $N = 1000$. Red dashed curves in panels (a1–a3, b1–b3) represent the analytical approximation given by Eqs. (7) and (8), respectively.

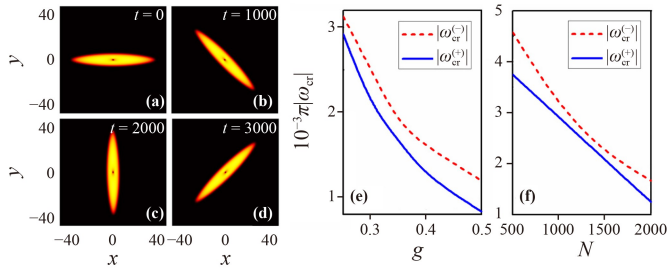

Fig. 3 **(a–d)** Steady spinning of 2D-AVQDs with $(N, g) = (1000, 0.25)$, which follows the rotation of the polarizing magnetic field with angular velocity $\omega = 0.25\pi \times 10^{-3}$. The shape of 2D-AVQDs is displayed at $t = 0$ (a), 1000 (b) 2000 (c), 3000 (d). **(e, f)** The largest angular velocities, $\left|\omega_{\rm cr}^{(\pm)}\right|$, which admit stable spinning of 2D-AVQDs in two opposite directions, vs. g (at $N = 1000$) and N (at $g = 0.25$), respectively.

In panels 2(b1, b2), both I_P and μ decay to zero at $g \to 2$. All the above numerical results agree well with the analytical predictions provided by Eqs. (7, 8). In panels 2(a3, b3) the effective area closely matches the analytical result [Eq. (7)]. In panels 2(a4, b4) the aspect ratio remains smaller than 0.25, which indicates that 2D-AVQDs manifest strong anisotropy with the elongation along the x-direction. For very strong anisotropy, viz., at $\mathcal{E}_l \leq 0.2$, relation $\bar{L}_z \approx 2\mathcal{E}_l$ roughly holds, which is explained by a straightforward estimate, $y\partial_x \sim W_y/W_x$, which is valid in this case.

Stationary 2D-AVQDs with higher vorticities, $S \geq 2$, have also been found in the numerical form. However, simulations demonstrate that they are fully unstable. For example, 2D-AVQDs with $S \geq 2$ can be generated by initiating the ITM with ansatz [Eq. (5)]. The result is splitting into an array of S unitary vortices set along the stretched axis of the AVQD. However, these composite vortex states are completely unstable.

3 Dynamics

It is known that zero-vorticity solitons in the dipolar BECs can rotate, adiabatically following slow in-plane rotation of the magnetic field which polarizes atomic magnetic moments [13]. The rotation can be introduced in Eq. (3) by replacing $\Theta \to \Theta + \omega t$. When the rotation is sufficiently slow, viz., $\omega < \omega_{\rm cr}$, 2D-AVQDs are able to follow it, in the state of spinning motion. Figures 3(a–d) show an example of the steady rotation of 2D-AVQDs. Numerical simulations demonstrate that $\omega_{\rm cr}$ decreases with the increase of the QD's size. Indeed, the large size makes it difficult to synchronize the rotational motion of the QD's core area and remote edges. The intrinsic vorticity of 2D-AVQDs makes it more tolerant to the rotation in the direction of the inner vorticity than against it, therefore the simulations demonstrate two different critical values, $\omega_{\rm cr}^{(\pm)}$, in Figs. 3(e, f).

Stable 2D-AVQDs can be set in motion by opposite kicks $\pm\eta$ applied along the x- or y-direction. Accordingly, it is possible to simulate collisions between 2D-AVQDs moving in opposite directions. Results demonstrate a drastic difference from the usual scenario of collisions in non-integrable systems with local nonlinearity, where the increase of η leads to a transition from inelastic collisions between slow solitons to quasi-elastic outcomes for fast ones [39]. In the present setting, elastic collisions are only observed between 2D-AVQDs moving in the y-direction if kick η is relatively small. If η is larger, or the head-on collision happens in other directions in the (x, y) plane, the outcome is inelastic, leading to merger of 2D-AVQDs with identical $(S_1 = S_2 = 1)$ or opposite $(S_1 = -S_2 = 1)$ vorticities into localized breathing modes. A noteworthy result is produced by the collision between 2D-AVQDs with $S_1 = S_2 = 1$ traveling in the x-direction (in which the dipoles are polarized): formation of a transient state in the form of a breathing vortex–antivortex–vortex structure. Eventually, this long-lived state transforms into a zero-vorticity breathing one. A typical example of such a collision is displayed in Fig. 4, where the central pivot, which represents the antivortex, emerges in the beginning of the merger of the two colliding vortices [see panels (b1, b2) in Fig. 4].

4 Vortex–antivortex–vortex bound states

The production of the above-mentioned long-lived vortex–antivortex–vortex breather by collisions along the x direction suggests that the system may support truly stationary bound states with a similar structure. They can indeed be produced by means of ITM, starting from a generalization of ansatz [Eq. (5)],

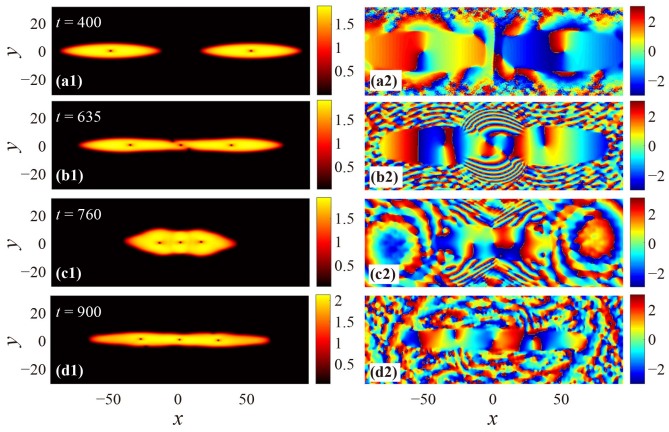

Fig. 4 The collision of two 2D-AVQDs with identical vorticities, initiated, at $t = 0$, by input $\phi(x - x_0, y)\mathrm{e}^{-\mathrm{i}\eta x} + \phi(x + x_0, y)\mathrm{e}^{\mathrm{i}\eta x}$ with $x_0 = 64$, $\eta = 0.025$, $g = 0.25$, and norm of each 2D-AVQDs $N = 1000$. **(a1–d1)** Density patterns at $t = 400$ (a1), 635 (b1), 760 (c1), and 900 (d1). **(a2–d2)** The corresponding phase diagrams for panels (a2–d2).

$$\phi^{(0)} = \sum_{\pm} A_{\pm}\tilde{r}_{\pm} \cdot \mathrm{e}^{-\alpha_{\pm}\tilde{r}_{\pm}^2 + \mathrm{i}\tilde{\theta}_{\pm}} + A\tilde{r}\mathrm{e}^{-\alpha\tilde{r}^2 - \mathrm{i}\tilde{\theta}}, \tag{10}$$

where $\tilde{r}_{\pm} \equiv \sqrt{(x \pm x_0)^2 + \beta^2 y^2}$, $\tilde{\theta}_{\pm} \equiv \arctan\left[\beta y/(x \pm x_0)\right]$, and x_0 is an appropriately chosen separation. A typical example of such a stable bound state is displayed in Figs. 5(a1, a2). The family of stable bound states is characterized by dependencies of the chemical potential on g and N, as shown in Figs. 5(b, c). In the latter panels, stable bound state of the vortex–antivortex–vortex type populate areas $g < 0.35$ and $900 < N < 2000$. Note also that the $\mu(N)$ relation satisfies the aforementioned VK criterion, $\mathrm{d}\mu/\mathrm{d}N < 0$. Similar to what is presented in Fig. 3, it is possible to apply a rotating magnetic field to the bound states of the present type, and test a possibility of their steady spinning motion, see Figs. 5(d1–d4).

5 Experimental scenarios

As mentioned above, dipole modes coexisting with the stable 2D-AVQDs in the chart displayed in Fig. 2(b) are unstable, rapidly transforming into stable vortex modes in the course of the perturbed real-time evolution, see an example in Fig. 6. This dynamical process suggests a promising way to create 2D-AVQDs in the experiment. Indeed, one can first produce an unstable dipole mode by imprinting a phase kink onto the fundamental QD, to be followed by its spontaneous transformation into the 2D-AVQDs. The phase-imprinting method is widely available, being used, in particular, to create dark solitons in BEC [40]. Spontaneous decay of quasi-1D dark solitons into delocalized vortices has been reported too [41]. A more sophisticated method for direct creation of vortex solitons may imprint the necessary phase pattern onto

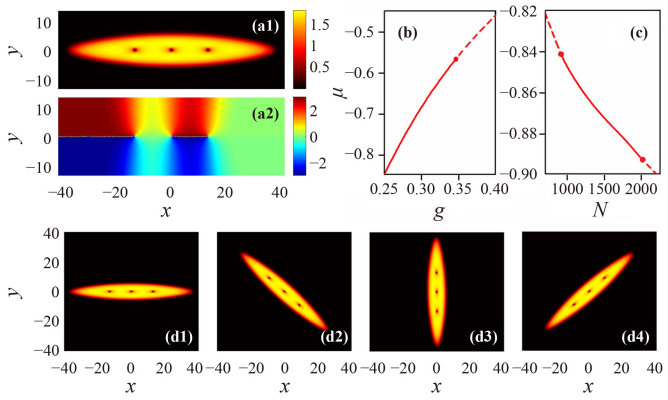

Fig. 5 **(a1, a2)** Density and phase patterns of the stable vortex–antivortex–vortex bound state with $(N, g) = (1000, 0.25)$, $x_0 = 13.6$ and $\mu = -0.8482$. **(b, c)** The chemical potential of the states of this type versus g (at $N = 1000$) and N (at $g = 0.25$), respectively. Solid and dashed parts of the curves represent, severally, stable and unstable states. **(d1–d4)** Steady spinning of a vortex–antivortex–vortex bound state with $(N, g) = (1000, 0.25)$, under the action of the polarizing magnetic field rotating with angular velocity $\omega = 0.2\pi \times 10^{-3}$. The shape of the bound state is displayed at $t = 0$ (d1), 1250 (d2) 2500 (d3), 3750 (d4).

fundamental QDs by vortical laser beams [42].

Finally, it is relevant to estimate physical parameters of the modes predicted in this work, with scaled norm N. Using the values of the magnetic moment for ^{164}Dy atoms and a typical transverse-confinement length, $a_{\perp} \sim 0.5$ μm [43–46], we conclude that the number of atoms in AVQDs is $N_{\mathrm{atom}} \sim 10N$, and the scaled length unit corresponds to ~0.1 μm.

6 Conclusion

We have constructed solutions for stable 2D-AVQDs in the effectively two-dimensional dipolar BEC. The anisotropy and stability are stipulated by the choice of the polarization of atomic dipoles parallel to the system' s plane and perpendicular to the vortex axis. The stability

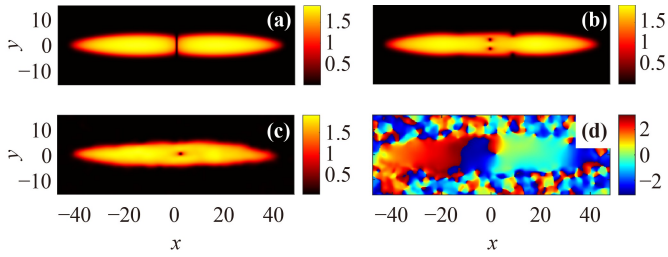

Fig. 6 **(a–c)** Spontaneous transformation of the unstable dipole mode with $N = 1000$ and $g = 0.25$ into a stable 2D-AVQDs is represented by density snapshots taken at $t = 0$ (a), 50 (b), and 700 (c). **(d)** The phase pattern at $t = 700$.

area of the 2D-AVQDs is identified in the system's parameter space. Characteristic features of the 2D-AVQDs, such as the peak density, chemical potential, effective area, aspect ratio, and average angular momentum, are presented. Spinning 2D-AVQDs can stably follow rotation of the polarizing magnetic field, provided that the rotation is not too fast. Collisions between slow or fast moving 2D-AVQDs are elastic or inelastic, respectively. In the latter case, the colliding 2D-AVQDs merge into breathers. In particular, these may be bound states of the vortex–antivortex–vortex type, which are also found as stable stationary states. An efficient method for the creation of the 2D-AVQDs in the experiment is to embed a phase kink into a zero-vorticity quantum droplet, letting it spontaneously transform into an 2D-AVQDs.

The present analysis can be extended further. First, it will be interesting to apply initial torque to an elongated 2D-AVQDs mode, and simulate ensuing dynamics, which is expected to feature oscillations of the droplet's orientation around the original elongated direction. Further, it may also be relevant to simulate the motion of a spinning 2D-AVQDs, driven by the rotating magnetic field, under the action of a kick. Another relevant possibility is to construct 2D-AVQDs in binary dipolar BECs, cf. Refs. [47, 48]. Finally, a challenging option is to seek for stable AVQDs in the full 3D setting.

Declarations The authors declare that they have no competing interests and there are no conflicts.

Acknowledgements This work was supported by the National Natural Science Foundation of China (NSFC) through Grant Nos. 12274077, 11874112, 12305013, and 11905032, the Natural Science Foundation of Guangdong Province through Grant Nos. 2021A1515010214 and 2021A1515111015, the Key Research Projects of General Colleges in Guangdong Province through Grant No. 2019KZDXM001, the Research Fund of Guangdong–Hong Kong–Macao Joint Laboratory for Intelligent Micro–Nano Optoelectronic Technology through Grant No. 2020B1212030010. The work of B.A.M. was supported, in part, by the Israel Science Foundation through Grant No. 1695/22.

References

1. G. Fibich and G. Papanicolaou, Self-focusing in the perturbed and unperturbed nonlinear Schrödinger equation in critical dimension, *SIAM J. Appl. Math.* 60(1), 183 (1999)
2. L. Bergé, Wave collapse in physics: Principles and applications to light and plasma waves, *Phys. Rep.* 303(5–6), 259 (1998)
3. E. A. Kuznetsov and F. Dias, Bifurcations of solitons and their stability, *Phys. Rep.* 507(2–3), 43 (2011)
4. B. A. Malomed, Two-dimensional solitons in nonlocal media: A brief review, *Symmetry (Basel)* 14(8), 1565 (2022)
5. B. A. Malomed, Multidimensional Solitons, American Institute of Physics: Melville, NY, 2022
6. R. Heidemann, U. Raitzsch, V. Bendkowsky, B. Butscher, R. Löw, and T. Pfau, Rydberg excitation of Bose–Einstein condensates, *Phys. Rev. Lett.* 100(3), 033601 (2008)
7. F. Maucher, N. Henkel, M. Saffman, W. Królikowski, S. Skupin, and T. Pohl, Rydberg-induced solitons: Three-dimensional self-trapping of matter waves, *Phys. Rev. Lett.* 106(17), 170401 (2011)
8. D. O'Dell, S. Giovanazzi, G. Kurizki, and V. M. Akulin, Bose–Einstein condensates with $1/r$ interatomic attraction: Electromagnetically induced "gravity", *Phys. Rev. Lett.* 84(25), 5687 (2000)
9. J. Qin, G. Dong, and B. A. Malomed, Stable giant vortex annuli in microwave-coupled atomic condensates, *Phys. Rev. A* 94(5), 053611 (2016)
10. T. Lahaye, C. Menotti, L. Santos, M. Lewenstein, and T. Pfau, The physics of dipolar bosonic quantum gases, *Rep. Prog. Phys.* 72(12), 126401 (2009)
11. P. Pedri and L. Santos, Two-dimensional bright solitons in dipolar Bose–Einstein condensates, *Phys. Rev. Lett.* 95(20), 200404 (2005)
12. R. Nath, P. Pedri, and L. Santos, Stability of dark solitons in three dimensional dipolar Bose–Einstein condensates, *Phys. Rev. Lett.* 101(21), 210402 (2008)
13. I. Tikhonenkov, B. A. Malomed, and A. Vardi, Anisotropic solitons in dipolar Bose–Einstein condensates, *Phys. Rev. Lett.* 100(9), 090406 (2008)
14. M. Raghunandan, C. Mishra, K. Lakomy, P. Pedri, L. Santos, and R. Nath, Two-dimensional bright solitons in dipolar Bose–Einstein condensates with tilted dipoles, *Phys. Rev. A* 92(1), 013637 (2015)
15. P. B. Blakie, Axial collective mode of a dipolar quantum droplet, *Photonics* 10(4), 393 (2023)
16. Y. Zhao, Y. Lei, Y. Xu, S. Xu, H. Triki, A. Biswas, and Q. Zhou, Vector spatiotemporal solitons and their memory features in cold Rydberg gases, *Chin. Phys. Lett.* 39(3), 034202 (2022)
17. I. Tikhonenkov, B. A. Malomed, and A. Vardi, Vortex solitons in dipolar Bose–Einstein condensates, *Phys. Rev. A* 78(4), 043614 (2008)
18. X. Jiang, Z. Fan, Z. Chen, W. Pang, Y. Li, and B. A. Malomed, Two-dimensional solitons in dipolar Bose-Einstein condensates with spin–orbit coupling, *Phys. Rev. A* 93(2), 023633 (2016)
19. B. Liao, Y. Ye, J. Zhuang, C. Huang, H. Deng, W. Pang, B. Liu, and Y. Li, Anisotropic solitary semivortices in dipolar spinor condensates controlled by the twodimensional anisotropic spin–orbit coupling, *Chaos Solitons Fractals* 116, 424 (2018)
20. B. Liao, S. Li, C. Huang, Z. Luo, W. Pang, H. Tan, B. A. Malomed, and Y. Li, Anisotropic semivortices in dipolar spinor condensates controlled by Zeeman splitting, *Phys. Rev. A* 96(4), 043613 (2017)
21. M. Schmitt, M. Wenzel, F. Böttcher, I. Ferrier-Barbut, and T. Pfau, Self-bound droplets of a dilute magnetic quantum liquid, *Nature* 539(7628), 259 (2016)
22. L. Chomaz, S. Baier, D. Petter, M. J. Mark, F. Wächtler, L. Santos, and F. Ferlaino, Quantum-fluctua-

tion-driven crossover from a dilute Bose–Einstein condensate to a macrodroplet in a dipolar quantum fluid, *Phys. Rev. X* 6(4), 041039 (2016)
23. C. R. Cabrera, L. Tanzi, J. Sanz, B. Naylor, P. Thomas, P. Cheiney, and L. Tarruell, Quantum liquid droplets in a mixture of Bose–Einstein condensates, *Science* 359(6373), 301 (2018)
24. G. Semeghini, G. Ferioli, L. Masi, C. Mazzinghi, L. Wolswijk, F. Minardi, M. Modugno, G. Modugno, M. Inguscio, and M. Fattori, Self-bound quantum droplets of atomic mixtures in free space, *Phys. Rev. Lett.* 120(23), 235301 (2018)
25. C. D'Errico, A. Burchianti, M. Prevedelli, L. Salasnich, F. Ancilotto, M. Modugno, F. Minardi, and C. Fort, Observation of quantum droplets in a heteronuclear bosonic mixture, *Phys. Rev. Res.* 1(3), 033155 (2019)
26. D. S. Petrov, Quantum mechanical stabilization of a collapsing Bose–Bose mixture, *Phys. Rev. Lett.* 115(15), 155302 (2015)
27. Z. Luo, W. Pang, B. Liu, Y. Li, and B. A. Malomed, A new kind form of liquid matter: Quantum droplets, *Front. Phys.* 16(3), 32201 (2021)
28. F. Böttcher, J. N. Schmidt, J. Hertkorn, K. S. H. Ng, S. D. Graham, M. Guo, T. Langen, and T. Pfau, New states of matter with fine-tuned interactions: Quantum droplets and dipolar supersolids, *Rep. Prog. Phys.* 84(1), 012403 (2021)
29. M. Guo and T. Pfau, A new state of matter of quantum droplets, *Front. Phys.* 16(3), 32202 (2021)
30. B. A. Malomed, The family of quantum droplets keeps expanding, *Front. Phys.* 16(2), 22504 (2021)
31. Y. Li, Z. Chen, Z. Luo, C. Huang, H. Tan, W. Pang, and B. A. Malomed, Two-dimensional vortex quantum droplets, *Phys. Rev. A* 98(6), 063602 (2018)
32. Y. V. Kartashov, B. A. Malomed, L. Tarruell, and L. Torner, Three-dimensional droplets of swirling superfluids, *Phys. Rev. A* 98(1), 013612 (2018)
33. X. Zhang, X. Xu, Y. Zheng, Z. Chen, B. Liu, C. Huang, B. A. Malomed, and Y. Li, Semidiscrete quantum droplets and vortices, *Phys. Rev. Lett.* 123, 113901 (2019)
34. A. Cidrim, F. E. A. dos Santos, E. A. L. Henn, and T. Macri, Vortices in self-bound dipolar droplets, *Phys. Rev. A* 98(2), 023618 (2018)
35. D. Baillie, R. M. Wilson, R. N. Bisset, and P. B. Blakie, Self-bound dipolar droplet: A localized matter wave in free space, *Phys. Rev. A* 94, 021602(R) (2016)
36. S. Sinha and L. Santos, Cold dipolar gases in quasi-one-dimensional geometries, *Phys. Rev. Lett.* 99(14), 140406 (2007)
37. J. Cuevas, B. A. Malomed, P. G. Kevrekidis, and D. J. Frantzeskakis, Solitons in quasi-one-dimensional Bose-Einstein condensates with competing dipolar and local interactions, *Phys. Rev. A* 79(5), 053608 (2009)
38. N. G. Vakhitov and A. A. Kolokolov, Stationary solutions of the wave equation in a medium with nonlinearity saturation, *Radiophys. Quantum Electron.* 16(7), 783 (1973)
39. Yu. S. Kivshar and B. A. Malomed, Dynamics of solitons in nearly integrable systems, *Rev. Mod. Phys.* 61(4), 763 (1989)
40. S. Burger, K. Bongs, S. Dettmer, W. Ertmer, K. Sengstock, A. Sanpera, G. V. Shlyapnikov, and M. Lewenstein, Dark solitons in Bose–Einstein condensates, *Phys. Rev. Lett.* 83(25), 5198 (1999)
41. B. P. Anderson, P. C. Haljan, C. A. Regal, D. L. Feder, L. A. Collins, C. W. Clark, and E. A. Cornell, Watching dark solitons decay into vortex rings in a Bose–Einstein condensate, *Phys. Rev. Lett.* 86(14), 2926 (2001)
42. Y. J. Shen, X. J. Wang, Z. W. Xie, C. J. Min, X. Fu, Q. Liu, M. L. Gong, and X. C. Yuan, Optical vortices 30 years on: OAM manipulation from topological charge to multiple singularities, *Light Sci. Appl.* 8(1), 90 (2019)
43. B. Ramachandhran, B. Opanchuk, X. J. Liu, H. Pu, P. D. Drummond, and H. Hu, Half-quantum vortex state in a spin–orbit-coupled Bose–Einstein condensate, *Phys. Rev. A* 85(2), 023606 (2012)
44. Y. Li, J. Liu, W. Pang, and B. A. Malomed, Matter-wave solitons supported by field-induced dipole–dipole repulsion with spatially modulated strength, *Phys. Rev. A* 88(5), 053630 (2013)
45. Y. Li, Y. Liu, Z. Fan, W. Pang, S. Fu, and B. A. Malomed, Two-dimensional dipolar gap solitons in free space with spin–orbit coupling, *Phys. Rev. A* 95(6), 063613 (2017)
46. C. Huang, Y. Ye, S. Liu, H. He, W. Pang, B. A. Malomed, and Y. Li, Excited states of two-dimensional solitons supported by spin–orbit coupling and field-induced dipole–dipole repulsion, *Phys. Rev. A* 97(1), 013636 (2018)
47. A. Boudjemâa, Fluctuations and quantum self-bound droplets in a dipolar Bose–Bose mixture, *Phys. Rev. A* 98(3), 033612 (2018)
48. R. N. Bisset, L. A. P. Ardila, and L. Santos, Quantum droplets of dipolar mixtures, *Phys. Rev. Lett.* 126(2), 025301 (2021)